

Development and experimental evaluation of grey-box models of a microscale polygeneration system for application in optimal control

Parantapa Sawant^{a,*}, Adrian Bürger^{b,c}, Minh Dang Doan^b, Clemens Felsmann^d, Jens Pfafferott^a

^a Institute of Energy Systems Technology (INES), Offenburg University of Applied Sciences, Offenburg, Germany

^b Systems Control and Optimization Laboratory, Department of Microsystems Engineering (IMTEK), University of Freiburg, Freiburg, Germany

^c Faculty of Management Science and Engineering, Karlsruhe University of Applied Sciences, Karlsruhe, Germany

^d Chair of Building Systems Engineering and Heat Supply, Technische Universität Dresden, Dresden, Germany

ARTICLE INFO

Article history:

Received 17 October 2019

Revised 16 December 2019

Accepted 23 December 2019

Available online 27 December 2019

Keywords:

Adsorption chiller model
Experimental validation of polygeneration system models
Grey-boxmodelling
Models for optimal control
Stratified thermal energy storage model

ABSTRACT

Optimisation based economic despatch of real-world complex energy systems demands reduced order and continuously differentiable component models that can represent their part-load behaviour and dynamic responses. A literature study of existing modelling methods and the necessary characteristics the models should meet for their successful application in model predictive control of a polygeneration system are presented. Deriving from that, a rational modelling procedure using engineering principles and assumptions to develop simplified component models is applied. The models are quantitatively and qualitatively evaluated against experimental data and their efficacy for application in a building automation and control architecture is established.

© 2019 Elsevier B.V. All rights reserved.

1. Introduction

Applying optimisation algorithms for the operation of decentralised polygeneration systems has shown promising results for their energy-efficient, sector-coupled (power-to-heat or gas-to-electricity) and grid-reactive scheduling [1–3]. Researchers have quantified potential economic benefits between 9.5% to 29% [4,5] by applying optimal control instead of conventional control to a wide range of polygeneration systems or to micro-grids utilising polygeneration systems. Also, a reduction of 50% in thermal energy wastage of a residential PV-trigeneration system [6] and upto 24% in primary energy consumption and CO₂ emissions of a 3.4 MW_{e1} trigeneration plant [7] is reported.

However, the common consensus in the research community regarding gaps in the status of optimum operation of microscale polygeneration systems available on the market is the lack of demonstration projects using advanced controllers like Model Predictive Control (MPC) [1,2,8]. The challenges lie in:

- lack of experimentally validated models that can simulate the wide range of non-linear operating conditions of such systems,

with sufficient accuracy and are yet simple enough for application in MPC,

- development and testing of a hierarchical control logic or architecture that combines the different levels of a Building Automation and Control (BAC) system.

This work contributes to the state-of-art in engineering research of optimal control for polygeneration systems by applying the grey-box methodology to program control-orientated models, and experimentally assesses their technical feasibility for implementation in an MPC.

A microscale polygeneration plant has been installed using standard industrial components at the Institute of Energy Systems Technology (INES) at Offenburg University of Applied Sciences. The absolute aim of the research project is to demonstrate MPC of this complex engineering system and the focus of this paper is the development and evaluation of the models essential for MPC. The procedure followed was:

- describing the experimental set-up and identifying the challenges for MPC-suitable models,
- establishing the state-of-art in modelling the respective components of the system,

* Corresponding author.

E-mail address: parantapa.sawant@hs-offenburg.de (P. Sawant).

Table 1
Important specifications of the main components.

Components	Abbr.	Specification
Adsorption chiller	AdC	12 kW _{th} cooling power max.; 0.65 max coefficient of performance
Combined heat and power unit	CHP	5 kW _{el} ; 10 kW _{th} ; 59% η _{th} ; 30% η _{el} ; fuel oil
Outdoor coil	OC	0.9 kW _{el} at 480 RPM
Reversible heat pump	RHP	12.9 kW _{th} (cooling power nom.); 16.7 kW _{th} (heating power nom.); 3.75 kW _{el} (power input nom.)
Thermal loads: Heating Load, Cooling Load	HL, CL	Circulation thermostats with precision temperature control (10 kW _{th} cooling and 18 kW _{th} heating power) and approx. 20 m ² of thermally activated building systems (ca. 3 kW _{th})
Thermal energy storage (water): Hot Tank, Chilled Tank	HT, CT	1500 l, 1450 l

- adapting the results of literature research to the grey-box methodology and developing the component-models to be used in MPC,
- comparing experimental and simulation results.

2. Problem description

The main specifications of the plant are given in Table 1 and details of the different operation modes are published in a previous work by the authors [9].

The control logic is summarised into the BAC for the plant as shown in Fig. 1 and consists of three levels: field level, automation level and management level.

It is planned to implement an economic-MPC as a supervisory controller on the management level using algorithmic differentiation and direct optimisation methods. At each sampling interval of 15 min, the mixed integer nonlinear program summarised in (1) will generate an optimal solution that minimises the operational costs formulated in (1a) over a 24-h prediction horizon. The switches of the four components will be formulated as the binary controls $b^T = [S_{CHP}, S_{AdC}, S_{HP}, S_{CC}]$ and constrained to either 0 or 1, shown in (1d).

$$\min_{x(\cdot), b(\cdot)} \int_{t_0}^{t_f} (\dot{v}_{Fuel}(t)Fuel_{price} + P_{el,Grid(buy)}(t)El_{buy}(t) - P_{el,Grid(sell)}(t)El_{sell}(t))dt \quad (1a)$$

subject to:

$$\dot{x}(t) - f(x(t), u(t), b(t), c(t), p(t)) = 0, \quad (1b)$$

$$h(x(t), u(t), b(t), c(t), s(t), p(t)) \leq 0, \quad (1c)$$

$$b(t) \in \{0, 1\}. \quad (1d)$$

The first element for each component switch from the entire optimal solution vector will be used as a control signal to generate the operation mode as per Table 2. The operation mode will be executed on the field level through the Human-Machine-Interface (HMI) on the automation level. The control loop will repeat at sampling intervals including the time needed for solving the algorithm and will use updated measurements and a new 24-h prediction horizon shifted by the sampling time length. The system dynamics and path constraints are considered in (1b) and (1c) respectively and will be captured by the models presented in this paper.

Consequently, the ability of the models to simulate with adequate accuracy and speed over the length of a 24-hour prediction horizon will greatly influence the quality (stability & practicality)

Table 2
Component switches for the seven possible operation modes, with Off = 0 and On = 1.

Operation mode	CHP	AdCM	HP	CC
1	Off	Off	Off	Off
2	On	Off	Off	Off
3	On	On	Off	Off
4	Off	Off	Off	On
5	Off	Off	On	Off
6	Off	On	Off	Off
7	On	Off	Off	On

of the supervisory controller. This ability is based on the sought after characteristics in the models (Fig. 2).

1a. Capture dynamic characteristics: When operating with actual components, a switch from one operating point to another often has a dynamic effect on the states of the system, and this should be included in the models for improving the controllability of the system [11]. In the context of MPC, if the components display slow dynamic behaviours extending far in excess of the sampling time interval, then this behaviour must be simulated accordingly.

1b. Capture part-load behaviour / internal control logic: Likewise, if the components operate at lower efficiencies under part-load or have an internal control logic that uses low-level controllers to improve their performance under part-load, then the applicable attribute should be simulated by the component models.

1c. Live parameterisation capabilities: If the MPC approach is to be integrated in a retrofit scenario, the rationale behind modelling the components should permit for live parameterisation. For example, regression-based models should use data that is readily collected in standard industrial practices and not data that needs specialised instrumentation or disassembly of the components.

1d. Generalisation capabilities: Likewise, if the MPC approach is to be integrated in a green-field scenario, the rationale behind modelling the components should permit for generalisation capabilities. For example, regression-based models should use data for fitting the coefficients that is readily available from standard component data sheets or can be collected during the commissioning phase of the plant.

1e. Adaptability to component design: In certain cases, the constructional design of the component influences its performance and its interoperability. An example of this in building energy systems is the construction of the storage tank. The height at which water enters and leaves the tank will depend on its hydraulic connections, or the type of heat transfer will depend on the heat exchanger installed in the tank. Thus, the models of such components should have the ability to adapt to the type of design.

2a. Lower complexity: In their paper on modelling and optimisation of a trigeneration system, Chandan et al., 2012 pointed out very clearly the unsuitability of detailed HVAC simulation models for direct use in an MPC structure due to their large computational times and other associated challenges [12]. For example, with each new system-state and time-varying parameter the size of the entire optimisation problem increases by a factor of the total number of sampling intervals over the entire forecast horizon, leading to an expansion of the state- and parameter spaces. The number of states and parameters in the component models should be limited to only those necessary for calculating outputs relevant for the particular optimisation problem.

2b. Sufficient accuracy: The required accuracy of models depends on the available system knowledge and on aspects of the real system that are relevant for accomplishment of the simulation objectives [13]. Considering this, the models needed for moving horizon MPC of thermal systems (which typically demonstrate slow dynamics) need to be only of sufficient accuracy since MPC gives

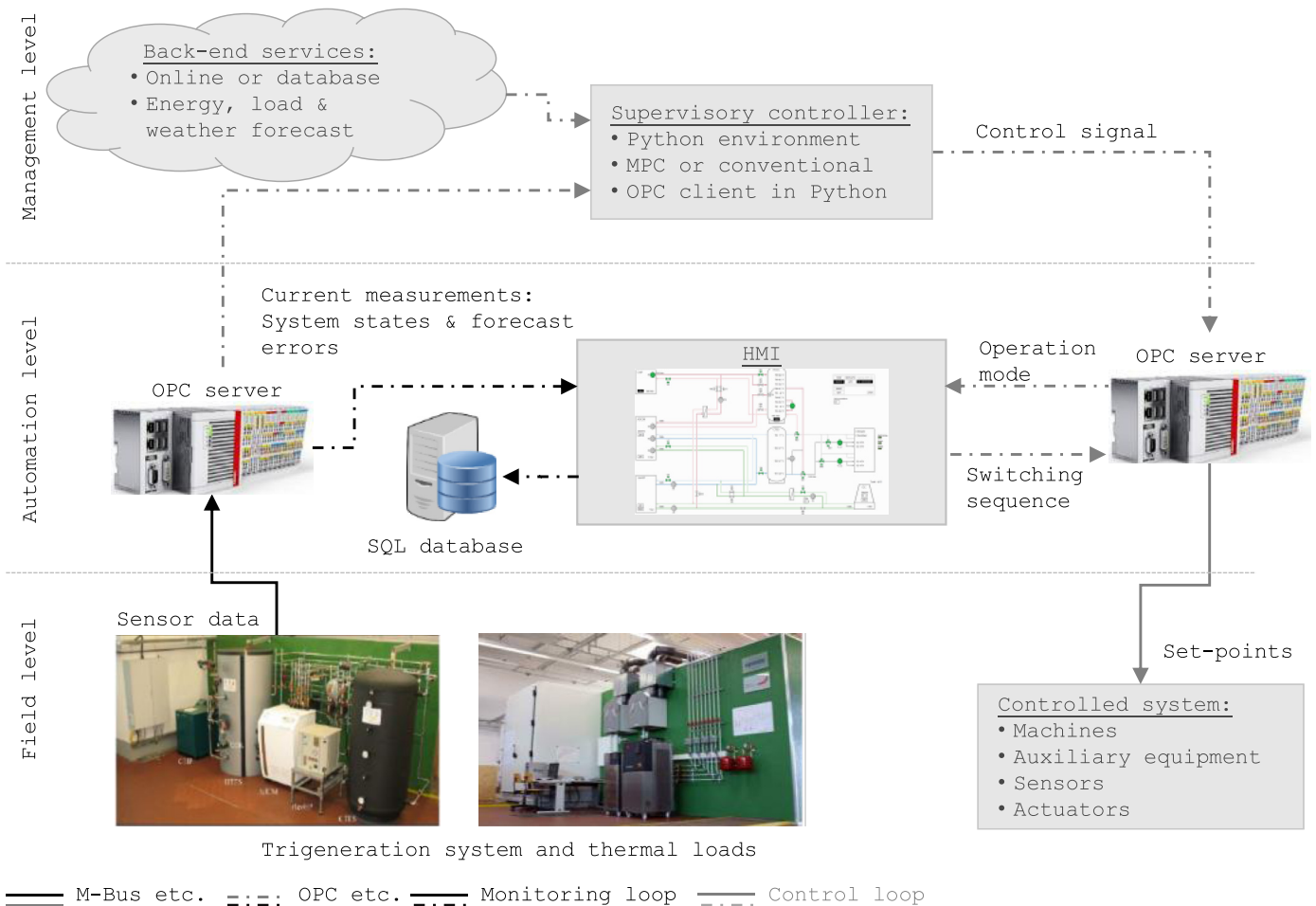


Fig. 1. Plan of the hierarchical control logic combining different levels of a BAC that will be used for optimal control of the microscale polygeneration plant at INES.

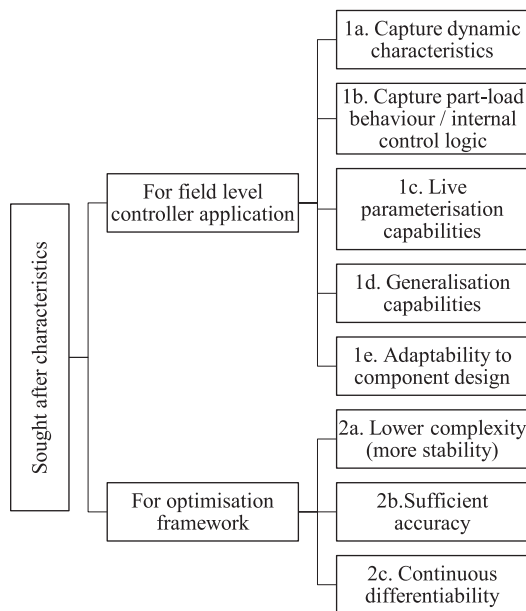


Fig. 2. Sought after characteristics of MPC-suitable models.

means to adjust the control and react to uncertainties or model-mismatch due to the update of system information after every sampling time [10,14].

2c. *Continuous differentiability*: The models need to be continuously differentiable when their application is in gradient-based optimisation methods [15].

3. Methodology

The state-of-the-art modelling techniques applied in the field of HVAC simulation and control were identified. Table 3 illustrates their classification to help analyse the different approaches and filter out the most relevant for this project. It was noticed that many simulation models for standard HVAC components were available and a further in-depth qualitative analysis of some selected approaches was done (Table 4).

In most cases the optimal scheduling problems consider only static process variables like electrical power or cooling capacities and do not consider dynamic states like storage temperatures or hydraulic circuit temperatures. On the other hand, existing models that satisfy these requirements are either physics-based models with a component level simulation focus making them very complex, or have rule-based controllers making them not continuously differentiable. Nevertheless, this analysis revealed important modelling features that were then adapted in this work.

Deriving from the qualitative analysis, from the results of previous functional tests [9] and from guidelines in literature reviews [13,16], the grey-box method was chosen to model the system. In grey-box modelling, the first law of thermodynamics and the principle of mass and energy balance is applied for developing the mathematical structure of the models and any missing vari-

Table 3
Illustration for HVAC modelling classification.

Modelling Class / Methodology	Main Outputs	Size/Complexity of Model	Objective of Study/Model and Validation	Reference(Years Ascending)	
AdC: Silica gel / water	<ul style="list-style-type: none"> Nonlinear dynamic white-box models LDF kinetic equation for adsorption and desorption rate Pressure and enthalpy based mass and energy balance Resistance-capacitance heat exchanger model and mass and energy balance 	CP, CT and COP	<ul style="list-style-type: none"> > 20 parameters > 4 states 2 curve fits 	To study the effects of circuit temperatures, switching time and cycle time on the AC performance Validation : Visual, quantitative (APE, RMSE, NSD)	[23,24]
CHP: Gas engine	<ul style="list-style-type: none"> Linear static grey-box models Linear interpolation or quadratic regression of predefined parameters for different load factors Energy balance 	Cost of operation, power, fuel	<ul style="list-style-type: none"> > 2 parameters 	Application in an MILP or MINLP for cost based optimisation to design and operate a CCHP system in a simulation environment Validation: NA	[25,26]
RHP: Compression chiller and heat pump	<ul style="list-style-type: none"> Nonlinear static grey-box models Parameter estimation from catalogue and experimental data Pressure-enthalpy based mass and energy balance over chiller internal components 	CP, PI,CT and COP	<ul style="list-style-type: none"> > 10 Parameters 	Deploy in energy calculation and/or building simulation programs to simulate detailed behaviour (including control logic) of an electric chiller Validation: Visual, quantitative (RMSE)	[27,28]
HT/CT: Stratified	<ul style="list-style-type: none"> 1-D dynamic multilayer model Fourier's equation for heat flow Mass and energy balance per layer If-else logic for charging/discharging Effective vertical heat conductivity 	Temperature distribution	<ul style="list-style-type: none"> 1 state per layer < 8 parameters 	Simulation of the transient temperatures in a stratified tank A simplified 2-layer model with 2 states per layer applied in nonlinear MPC for scheduling of a chiller plant in a simulation environment. Validation : Visual	[29,30]

AE (Absolute Error), APE (Absolute Percentage Error), CCHP (Combined Cooling Heating and Power), COP (Coefficient of Performance), CP (Cooling Power), CT (Circuit Temperatures), DAE (Differential Algebraic Equations), DP (Dynamic Programming), DSH (District Heating), GSHP (Ground Source Heat Pump), LDF (Linear Driving Force), MAE (Mean Absolute Error), MAPE (Mean Absolute Percentage Error), MILP (Mixed Integer Linear Program), MINLP (Mixed Integer Nonlinear Program), NA (Not Available), NLP (Nonlinear Program), NSD (Normalised Standard Deviation), NTU (Number of Transfer Units), PI (Power Input), RMSE (Root Mean Squared Error), RMSRE (Root Mean Squared Relative Error).

Table 4
Qualitative analysis of shortlisted models.

Reference (Years Ascending)	Component Dynamics	Part-Load Behaviour or Internal Control Logic	Live Parameter Identification Capabilities	Accuracy	Continuous Differentiability	Generalisation Capabilities	Adaptability to Component Design	Complexity
AdC [23]	Yes	Yes / Yes	No	Very high	Yes	Medium	-	Very high
[24]	Yes	Yes / Yes	No	Very high	Yes	Medium	-	Very high
[31]	No	No / No	No	Very low	Yes	Low	-	Very low
CHP [25]	No	Yes / No	No	High	Yes	Medium	-	Low
[32]	Yes	No / No	Yes	Very high	Yes	Low	-	Low
[33]	Yes	Yes / Yes	Yes	High	Yes	High	-	High
RHP [27]	No	Yes / -	No	High	Yes	Medium	-	High
[30]	No	Yes / -	No	High	Yes	Medium	-	Medium
[34]	No	Yes / -	Yes	High	Yes	High	-	Medium
[35]	No	Yes / -	No	Very high	Yes	Low	-	Low
HT [29]	Yes	-	-	High	No	Medium	No	Medium
[36]	Yes	-	-	Low	No	High	No	Low
[30]	Yes	-	-	Low	No	High	No	Low

ables or unknown physical processes are quantified through data fitting methods. This method is a compromise between physics-based white-box models and data-driven black-box models and can provide good generalisation capabilities while maintaining a high level of accuracy [16–18]. Grey-box models are also robust to disturbances, have auto-tuning capabilities, and need fewer assumptions to set-up. This is an advantage over data-driven algorithms like artificial neural networks for developing black-box models that show accurate results but have limited generalisation capabilities and less robustness to disturbances [19].

For the grey-box modelling approach, regression analysis [20] and step-response analysis [21] were used for fitting a priori data and determining the dynamic properties of the components. Both these methods make it possible for the user to choose data sets that are either readily available in the manufacturer's catalogues or can be collected during commissioning of the equipment. For regression analysis, the generalised reducing gradient search (via Microsoft Excel's Data Solver®) algorithm was applied and for step-response analysis, the "Control Design and Simulation Module" in LabVIEW® was used.

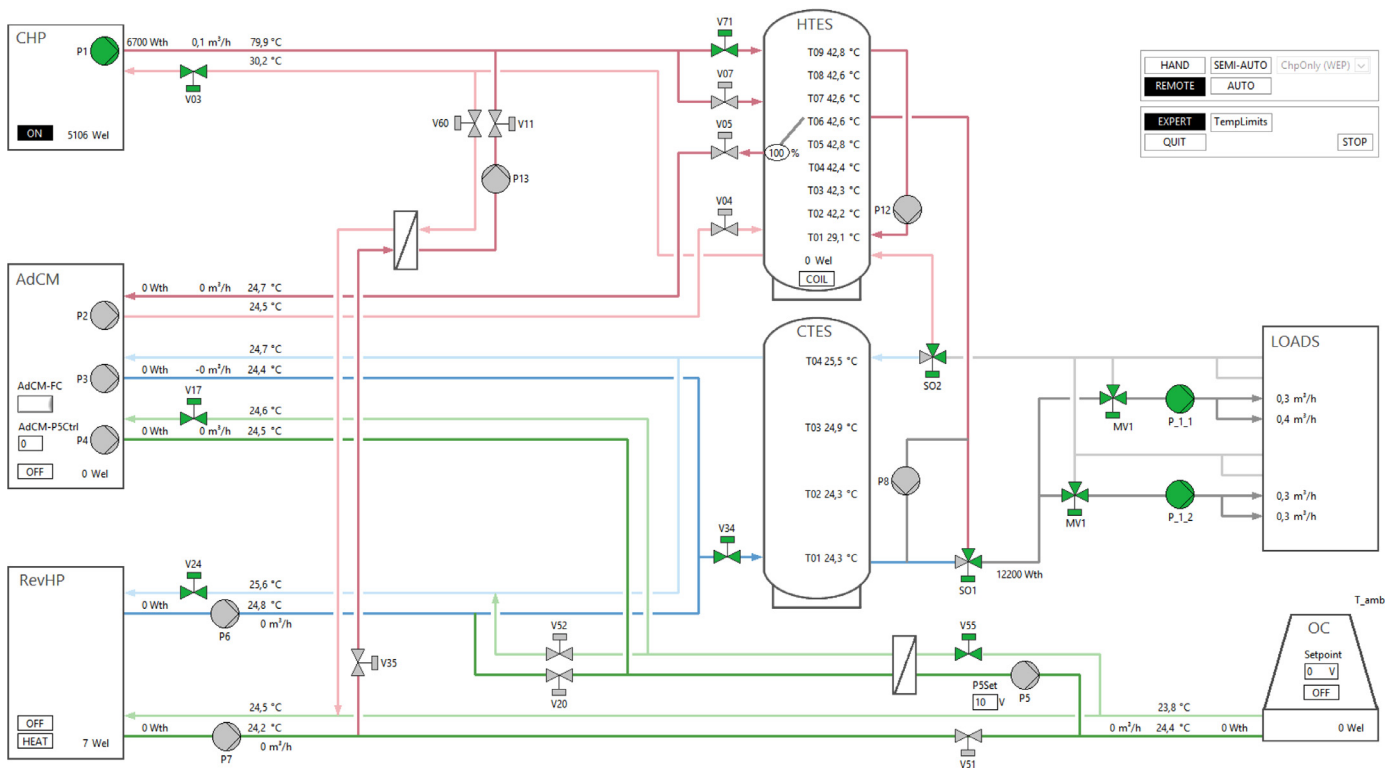


Fig. 3. Process flow diagram of the INES polygeneration system.

The models are developed in OpenModelica as input / output equations for the individual components using elemental libraries like SI Units and connectors [22]. They are then integrated into a system simulation model shown representatively as a process flow diagram in Fig. 3. Nomenclature from process engineering is followed, wherein flows leaving a component are designated *feed-line* (subscript “f”), and flows entering a component are designated *return-line* (subscript “r”). In addition, *high temperature circuit* is denoted with a “(H)”, *medium temperature circuit* with “(M)”, and *low temperature circuit* with “(L)”.

4. Models of the primary components

For the modelling of this complex energy plant, certain general and component specific simplifying assumptions, founded on engineering know-how and apriori knowledge of the system were made. The general assumptions were:

- Heat losses and pressure losses through pipes and components (other than storage tanks) were neglected,
- specific heats and densities of all fluids were assumed constant,
- ideal conservation of mass was assumed,
- at full load real power is the nominal power of the equipment,
- internal controllers of components are ideal and reliable,
- volume flows in the circuits are constant (other than for CHP and loads) and maintained at nominal flows,

accurate forecast of ambient temperature and building thermal loads are available over the entire simulation horizon. The mass flow \dot{m} (kg/s) in a machine’s hydraulic circuit is computed depending on the machine’s operation status as follows (2):

$$\dot{m} = S \frac{\dot{v}\rho}{3600} \quad (2)$$

Where, S is the on-off switch for the corresponding machine and a binary control variable in the optimisation problem, \dot{v} is the volume flow (m³/h) and ρ is the density of the fluid (kg/m³).

This formulation has two advantages; firstly, when the machines are switched off, then no mass flow occurs between components and storage tanks ensuring that storage-temperatures are not affected. Secondly, the decision variables occur a reduced number of times in the MPC formulation itself since they are avoided in the mass and energy balance equations for the individual models as shown in the following sections.

4.1. Adsorption Chiller (AdC) model

An AdC operates on the principle of sorption of solids (adsorption) like silica-gel and the cooling effect is produced by an adsorption triggered evaporation. To produce continuous cooling effectively, the machine has two adsorbing chambers that undergo the adsorption/desorption and heat recovery phases inversely. Hot water is used to drive the desorption process of a charged adsorber. The desorbed refrigerant (water) is condensed by removing the heat to the environment. Concurrently, the cooling load evaporates the refrigerant and is led to the adsorber. The exothermic heat of adsorption is also expelled together with the heat of liquefaction to the environment. After end of one adsorption/desorption phase a heat recovery phase occurs and then the roles of the modules reverse. This operation is achieved through internal switching of valves and pumps using complex control algorithms leading to the distinctive cyclic behaviour of the three circuit temperatures, as reported in literature [37]. The modelling of this internal dynamics has been included in some models as shown in Table 3. However, the complexity of these models makes them ineffective for a system-wide optimisation. On the other extreme, a highly simplified linear energy balance model that assumes a constant Coefficient of Performance (COP) does not capture the part-load behaviour of the machine, which is highly dependant on its inlet temperatures [31]. As seen in Section 2, a balance of complexity and accuracy must be achieved to develop a practical AdC model that is part of an entire system being optimally scheduled.

Based on previous experimental work and literature research, the following important simplifying assumptions for the modelling of this component were established [9,38]:

- for typical AdC based trigeneration systems, adequate storage (hot and cold) capacity is often planned and these smoothen the cyclic temperature pattern due to their damping effect making it unnecessary to model this pattern in detail,
- the heat released to the environment over an entire cycle $Q_{th,AdC(M)}$ is approximately equal to the sum of driving heat $Q_{th,AdC(H)}$ and the cooling energy $Q_{th,AdC(L)}$ over that cycle,
- manufacturer's catalogues of widely used industrial AdCs provide characteristic curves for cooling power and COP depending on inlet temperatures in the three circuits.

Considering the above findings and assumptions, regression analysis was applied to fit the cooling power and COP of the AdC as second order functions of the three inlet temperatures as shown in (3) and (4).

$$P_{th,AdC(L)} = d_1 + d_2 T_{r,AdC(L)} + d_3 T_{r,AdC(H)} + d_4 T_{r,AdC(M)} + d_5 T_{r,AdC(L)}^2 + d_6 T_{r,AdC(H)}^2 + d_7 T_{r,AdC(M)}^2 + d_8 T_{r,AdC(L)} T_{r,AdC(H)} + d_9 T_{r,AdC(L)} T_{r,AdC(M)} + d_{10} T_{r,AdC(H)} T_{r,AdC(M)} \quad (3)$$

$$COP = e_1 + e_2 T_{r,AdC(L)} + e_3 T_{r,AdC(H)} + e_4 T_{r,AdC(M)} + e_5 T_{r,AdC(L)}^2 + e_6 T_{r,AdC(H)}^2 + e_7 T_{r,AdC(M)}^2 + e_8 T_{r,AdC(L)} T_{r,AdC(H)} + e_9 T_{r,AdC(L)} T_{r,AdC(M)} + e_{10} T_{r,AdC(H)} T_{r,AdC(M)} \quad (4)$$

Applying previous assumptions and definition of COP the power balance over the three circuits was done as per (5) and (6).

$$P_{th,AdC(H)} = \frac{P_{th,AdC(L)}}{COP} \quad (5)$$

$$P_{th,AdC(M)} = P_{th,AdC(H)} + P_{th,AdC(L)} \quad (6)$$

Using the calculated thermal powers and applying the first law of thermodynamics, the feed-line temperatures for each circuit were calculated as in (7),(8) and (9).

$$T_{f,AdC(L)} = T_{r,AdC(L)} - \frac{P_{th,AdC(L)}}{\frac{\rho_w}{3600} \dot{V}_{AdC(L)} c_{p,w}} \quad (7)$$

$$T_{f,AdC(M)} = T_{r,AdC(M)} - \frac{P_{th,AdC(M)}}{\frac{\rho_w}{3600} \dot{V}_{AdC(M)} c_{p,w}} \quad (8)$$

$$T_{f,AdC(H)} = T_{r,AdC(H)} - \frac{P_{th,AdC(H)}}{\frac{\rho_w}{3600} \dot{V}_{AdC(H)} c_{p,w}} \quad (9)$$

The volume flows in the three circuits $\dot{V}_{AdC(L)}$, $\dot{V}_{AdC(M)}$, and $\dot{V}_{AdC(H)}$ are constant parameters of the model. When the machines are turned off, a division by zero is avoided by using these constant volume flows instead of mass flows in the equations above. The actual mass flows are calculated using (2) and are zero when the machines are off.

AdC's electric consumption was calculated with (10).

$$P_{el,AdC} = S_{AC} P_{el,AdC(Nom)} \quad (10)$$

4.2. Combined Heating and Power (CHP) model

The CHP comprises of a single cylinder engine coupled to an asynchronous generator that together convert fuel into thermal $P_{th,CHP}$ and electrical power $P_{el,CHP}$. The heat is transferred to the cooling water of the CHP, which flows in a closed circuit connected to the stratified Hot Tank (HT). Cold water coming from the bottom of the HT enters in the return-line of the CHP with $T_{r,CHP}$ and hot

water leaving the CHP at $T_{f,CHP}$ enters in the feed-line and is added to the top of the HT. An embedded controller in the CHP maintains the following internal control logic:

- volume flow of water \dot{V}_{CHP} is controlled depending on return line temperature $T_{r,CHP}$ to minimise part-load losses
- start-up checks needing 25 s (introduce delay time of approx. 25 s).

Further analysis of the CHP-functional tests showed slow first-order dynamics for the $P_{th,CHP}$ during start-up [9].

Most models used in literature for optimisation do not integrate this control logic or dynamic behaviour and are typically linear fits of apriori data. Some models use the black-box approach requiring many high quality data sets for parameterisation thus making it difficult to generalise the models for other systems. Another approach is to represent the dynamic behaviour through a mass and energy balance over the engine block and the heat exchanger, thereby increasing the number of system states and parameters (complexity) for modelling the CHP.

Founded on previous experimental work and literature research, following important simplifying assumptions were established:

- the delay time after start-up can be neglected since the length of the sampling time and forecast horizon for a 15-minute electricity price based MPC is significantly larger than the delay time interval itself,
- the internal control logic for \dot{V}_{CHP} can be portrayed using the regression-based approach where it is fit to the incoming $T_{r,CHP}$ using a second order univariate linear regression [33],
- the dynamic behaviour of the thermal power $P_{th,CHP}$ can be portrayed using a differential equation obtained by the step-response analysis method [32],
- internal control logic of the modern day CHPs and their operation in combination with a storage and other components ensure close to full-load operation. Therefore, if this logic is included in the model, it is not necessary to simulate the part-load operation separately and constant efficiencies can be assumed for optimisation problems [11],
- Higher Calorific Value (HCV) of fuel is used for calculation,
- a complete combustion of fuel occurs in the CHP.

Considering the above findings and assumptions, the internal controller and dynamic behaviour of the CHP were modelled as shown in (11) and (12) respectively.

$$\dot{V}_{CHP} = b_1 + b_2 T_{r,CHP} + b_3 T_{r,CHP}^2 \quad (11)$$

$$\frac{dP_{th,CHP}}{dt} = \frac{P_{th,CHP(Nom)} S_{CHP} - P_{th,CHP}}{c_1} \quad (12)$$

Here c_1 represents the average time constant (in seconds) of the CHP system that was determined by performing a step-response analysis over three tests with varying initial temperatures.

Using the calculated thermal power and volume flow and applying the first law of thermodynamics the feed-line temperature was calculated as in (13)

$$T_{f,CHP} = T_{r,CHP} + \frac{P_{th,CHP}}{\frac{\rho_w}{3600} \dot{V}_{CHP} c_{p,w}} \quad (13)$$

The mass flow going to the HT was calculated using (2) shown earlier and the electrical production of the CHP $P_{el,CHP}$ is given in (13) below:

$$P_{el,CHP} = S_{CHP} P_{el,CHP(Nom)} \quad (14)$$

Furthermore, the fuel consumed by the CHP was calculated using (15). This formulation aids in generalising the type of fuel that could be used in the simulation.

$$\dot{V}_{Fuel} = S_{CHP} \frac{P_{el,CHP(Nom)} + P_{th,CHP(Nom)}}{HCV_{Fuel} (\eta_{el(Nom)} + \eta_{th(Nom)})} \quad (15)$$

4.3. Outdoor Coil (OC) and Heat Exchanger(hx) model

The OC and HX models were derived from the “Number of Transfer Units – Effectiveness (NTU- ε)” method [39]. The NTU- ε method calculates the effectiveness of a heat exchanger depending on the maximum possible heat transfer that can be hypothetically achieved.

The OC is the heat-sink for the condenser of the chilling machines and the heat-source for the evaporator of the heat pump (cf. Fig. 3). It is principally a dry-cooling tower with three variable-speed fan motors consuming a total $P_{el,OC,max}$ of 0.9 kW_{el} at their maximum speed, RPM_{max} of 480 RPM.

Other assumptions for this model are:

- homogeneous air flow,
- negligible effect of the instantaneous variations of air speed on the pressure,
- no pressure loss over the heat exchangers.

By means of NTU- ε method and with energy balance over the OC the fluid outlet temperature was calculated from (16). Where, ε is the effectiveness of a cross-flow heat exchanger, C_{min} is smaller of the two fluid heat capacity rates and C_h is the heat capacity rate of the hot fluid.

$$T_{f,OC} = T_{r,OC} - \frac{\varepsilon C_{min}(T_{r,OC} - T_{Amb})}{C_h} \quad (16)$$

Additionally, assuming a constant efficiency and fan diameter, the “Fan Affinity Laws” were applied to simulate the relationship between the RPM and electrical power consumed by the OC $P_{el,OC}$ as seen in (17) [39].

$$P_{el,OC} = S_{OC} \frac{RPM^3 P_{el,OC(max)}}{RPM_{max}^3} \quad (17)$$

4.4. Reversible heat pump (RHP) model

The RHP can operate as a Heat Pump (HP) or as a Compression Chiller (CC) and is principally a conventional refrigeration system operating on the vapour-compression cycle [34]. The switching in their operation is done over external hydraulic connections from the evaporator/condenser to the OC. The *evaporator circuit* and *condenser circuit* are designated with subscript “e” and “c” respectively. During HP mode the evaporator circuit has medium temperature and condenser circuit has high temperature. During CC mode the evaporator circuit has low temperature and condenser circuit has medium temperature.

In the literature study, modelling approaches were identified that use manufacturer’s data tables or data that is readily available during the commissioning of these machines Table 3). Second order equations like ((18),(19) and (20) were fit by performing polynomial regression of manufacturer’s data tables, for calculating the heating power $P_{th,HP(H)}$, cooling power $P_{th,CC(L)}$ and power consumption $P_{el,RHP}$ respectively. $P_{el,RHP}$ was calculated based on the evaporator and condenser inlet temperatures of the particular mode. The equations capture the part-load behaviour of the machine as a function of the inlet temperatures.

$$P_{th,HP(H)} = g_1 + g_2 T_{r,HP(H)} + g_3 T_{r,HP(M)} + g_4 T_{r,HP(H)} T_{r,HP(M)} + g_5 T_{r,HP(H)}^2 + g_6 T_{r,HP(M)}^2 \quad (18)$$

$$P_{th,CC(L)} = h_1 + h_2 T_{r,CC(M)} + h_3 T_{r,CC(L)} + h_4 T_{r,CC(M)} T_{r,CC(L)} + h_5 T_{r,CC(M)}^2 + h_6 T_{r,CC(L)}^2 \quad (19)$$

$$P_{el,RHP} = S_{RHP}(i_1 + i_2 T_{r,RHP(e)} + i_3 T_{r,RHP(c)} + i_4 T_{r,RHP(e)} T_{r,RHP(c)} + i_5 T_{r,RHP(e)}^2 + i_6 T_{r,RHP(c)}^2) \quad (20)$$

Assuming an ideal refrigeration cycle, the power balance for the RHP in the HP mode was calculated by (21) and in the CC mode by (22) [40].

$$P_{th,HP(M)} = P_{th,HP(H)} - P_{el,RHP} \quad (21)$$

$$P_{th,CC(M)} = P_{th,CC(L)} + P_{el,RHP} \quad (22)$$

The first law of thermodynamics was applied in each circuit to get the feed-line temperatures as shown below for the HP condenser circuit and the CC evaporator circuit:

$$T_{f,HP(H)} = T_{r,HP(H)} + \frac{P_{th,HP(H)}}{\frac{\rho_w}{3600} \dot{V}_{HP(H)} c_{p,b}} \quad (23)$$

$$T_{f,CC(L)} = T_{r,CC(L)} - \frac{P_{th,CC(L)}}{\frac{\rho_w}{3600} \dot{V}_{CC(L)} c_{p,w}} \quad (24)$$

Where, $c_{p,b}$ and $c_{p,w}$ are the specific heat capacities of brine and water respectively.

4.5. Thermal energy storage (HT & CT) model

Thermal storage helps to balance out the mismatch in the production and consumption cycles especially in variable renewable energy systems. The modelling of such storage is complex due to physical effects of thermal stratification, forced convection or laminar flows that may occur depending on the construction of the tank. The simulation of the stratification effects is important especially when performing cost-based operational optimisation [41], as stratification is closely linked with the dynamic operation of the plant and its simulation increases the accuracy of the tank model. In the literature (Table 3 & Table 4), mixed storage tanks or no storage tanks are mostly used for design-optimisation of energy systems. However, it is highly recommended to apply at least a simple stratified tank model in optimal control problems [42].

The model of the thermal storage tanks in this work was adapted from a 1-D dynamic multilayer model using the Fourier’s equation [29,43]. This analytical model summarises the complex thermal flux using an effective vertical heat conductivity coefficient λ_{eff} . Here, the HT is considered as a vertically stratified cylindrical tank as shown in Fig. 4 with user defined dimensional parameters such as the diameter D , height H , thickness of tank wall Th and number of layers in the longitudinal direction N . An effective mass flow \dot{m}_i for each layer is calculated depending on the balance of mass flows from the *source circuit* (subscript “s”) and *load circuit* (subscript “l”). If \dot{m}_i is positive, then energy flows from the layer above the i^{th} layer ($i + 1$) and is interpreted by the binary parameter $\delta_i^+ = 1$, else $\delta_i^+ = 0$. A negative \dot{m}_i signifies mass flow from

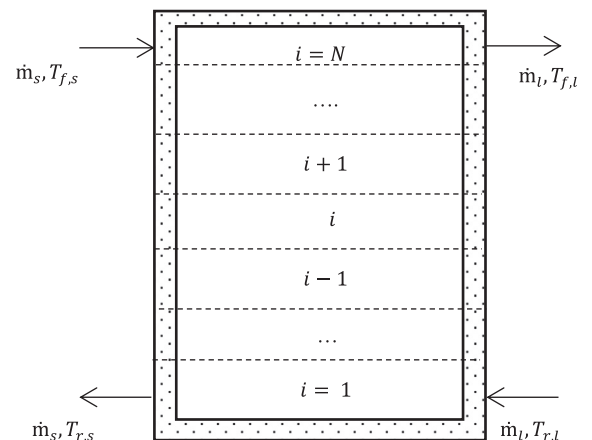


Fig. 4. Schematic depiction of the HT with hydraulic connections and layer numbering.

layer below the i^{th} layer, i.e. \dot{m}_i is greater than \dot{m}_s and thus cooling of the i^{th} layer occurs. It is considered by the parameter δ_i^- . Only for the top most layer (N^{th} layer) with hot water entering from the feed-line of the source circuit, the parameter δ_i^s is equal to 1 and analogously for the bottom most layer (1st layer) with cooler water entering from the return-line of the load circuit the parameter δ_i^l is equal to 1. From the user defined dimensional parameters of the tank, other relevant dimensional quantities such as the exterior heat transfer surface area of a layer $A_{\text{ext},i}$, cross-section area of a layer A_i , mass of a layer m_i and height of a layer z_i are calculated as follows:

$$z_i = H/N \quad (25)$$

$$A_{\text{ext},i} = \pi D z_i \quad (26)$$

$$A_i = \pi (D - 2Th)^2 / 4 \quad (27)$$

$$m_i = A_i z_i \rho_w \quad (28)$$

The general energy balance of each layer is then calculated as shown in.

$$\begin{aligned} m_i c_p \frac{dT_i}{dt} = & \delta_i^s (\dot{m} c_p)_s (T_{f,s} - T_i) - \delta_i^l (\dot{m} c_p)_l (T_i - T_{r,l}) \\ & - k A_{\text{ext},i} (T_i - T_{\text{amb}}) + \delta_i^+ \dot{m}_i c_p (T_{i+1} - T_i) \\ & + \delta_i^- \dot{m}_{i+1} c_p (T_i - T_{i-1}) + \frac{A_i \lambda_{\text{eff}}}{z_i} (T_{i+1} - 2T_i + T_{i-1}) \end{aligned} \quad (29)$$

where,

T_i - temperature of i^{th} layer (°C)

k - overall heat transfer coefficient of the tank envelope (W/(m²·K))

λ_{eff} - effective vertical heat conductivity of water (W/(m·K))

However, the limitations of this approach for application in the current scenario are as follows:

- **Differentiability:** Within gradient-based optimisation methods, models must be continuous and differentiable [38]. The presence of "If-Else"-statements within models introduces discontinuities and must therefore be avoided.

The formulation of the energy balance for each layer was modified to avoid the "If-Else" condition and replaced with a continuous and smooth formulation shown in (30).

$$\begin{aligned} m_i c_p \frac{dT_i}{dt} = & \delta_i^s (\dot{m} c_p)_s (T_{f,s} - T_i) - \delta_i^l (\dot{m} c_p)_l (T_i - T_{r,l}) \\ & - k A_{\text{ext},i} (T_i - T_{\text{amb}}) + \frac{\dot{m}_i c_p (a+B)}{2} + \frac{(\sqrt{\dot{m}_i^2 + \omega}) c_p (a-B)}{2} \\ & + \frac{A_i \lambda_{\text{eff}}}{z_i} (T_{i+1} - 2T_i + T_{i-1}) \end{aligned} \quad (30)$$

where,

$$a = T_{i+1} - T_i$$

$$B = T_i - T_{i-1}$$

$$\omega \in \mathbb{R} \text{ and } \omega \ll \dot{m}_i.$$

For $\dot{m}_i > 0$, the part " $\frac{\dot{m}_i c_p (a+B)}{2} + \frac{(\sqrt{\dot{m}_i^2 + \omega}) c_p (a-B)}{2}$ " will take the value $\approx \dot{m}_i c_p a$

For $\dot{m}_i < 0$ the part " $\frac{\dot{m}_i c_p (a+B)}{2} + \frac{(\sqrt{\dot{m}_i^2 + \omega}) c_p (a-B)}{2}$ " will take the value $\approx -\dot{m}_i c_p B$

In this study, the \dot{m}_i was in the range of 0.02 kg/s and 0.69 kg/s and a value of 2×10^{-4} is presumed for ω . For a well-insulated steel tank k and λ_{eff} were assumed to be 0.002 W/(m²·K) and 0.0015 W/(m·K) respectively [29]. With a given initial temperature distribution, the differential equation is applied to each layer and integrated over the entire forecast horizon to calculate the analytical temperature distribution over that time period.

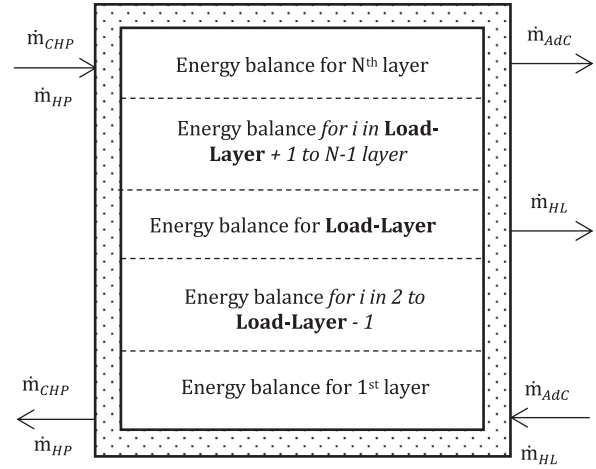


Fig. 5. Modification of tank model based on numerical loops to include a user-defined parameter "Load-Layer".

- **Component design:** For simplification purposes, the model in literature assumed that the hot source water enters at the top of the tank and is delivered to the load from the top of the tank. Similarly, the bottom of the tank is connected to the source and load circuits. However, in this experimental set-up, the construction of the HT has hydraulic connections at different heights of the tank making the simple assumption impractical. To improve the capability of the model to simulate the temperature distribution accurately and adapt the model to different constructions the formulation of the energy balance over the length of the tank was modified by introducing a user-defined parameter "Load-Layer" [40].

This acts as a tank splitting parameter and represents the layer from which water goes to the thermal loads. A differential equation is created for each section of the tank by implementing "For-loops" as shown in Fig. 5. Thus, by using an additional parameter a particular hydraulic connection was included in the model. This technique could be extended to multiple hydraulic connections at different heights of the tank.

The model of the CT was similarly developed but adapted to the reversal of flows between the source and load circuits. The tank models were discretised into 10 layers for each temperature sensor (90 discretisations for HT and 40 discretisations for CT).

4.6. Thermal loads (HL & CL) model

Since the thermal loads are perfectly forecasted and are generated using the thermostats, test chambers, and mixing valves, the models for the loads are developed by applying the first law of thermodynamics and the law of fluid mixing. The temperature of water at "Load-Layer" in the HT is fed to the mixing valve $T_{f,HL}$ which then mixes the necessary amount of return line water to achieve set feed line temperature for the HVAC distribution element $T_{f,HVAC}$.

Under following assumptions:

- the feed line temperature $T_{f,HVAC}$ and mass flow \dot{m}_{HVAC} in the HVAC circuit is constant,
- the temperature of water returning to the tank is the same as temperature leaving the HVAC distribution element,

the mass of water taken from the HT for covering the heating load $P_{th,HL}$ was calculated using (31):

$$\dot{m}_{HL} = \frac{P_{th,HL} \dot{m}_{HVAC}}{\dot{m}_{HVAC} c_{p,w} (T_{f,HL} - T_{f,HVAC}) + P_{th,HL}} \quad (31)$$

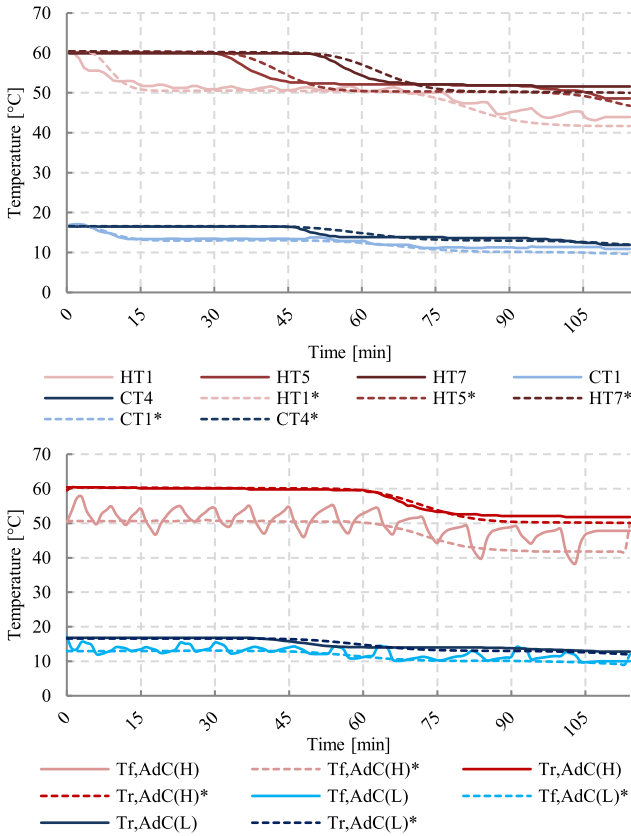


Fig. 6. Experimental and simulation data for the SEP mode. (a) Tank temperatures. (b) AdC circuit temperatures. Measured values (solid lines) and simulation results (*dashed lines).

Similarly, the mass flow from CT \dot{m}_{CL} to cooling load $P_{th,CL}$ was calculated from an energy balance in the cooling circuit.

5. 5. model evaluation results

Comprehensive evaluation of the models' performance was done using extensive empirical tests with varying ambient temperatures, initial tank temperatures, load profiles and control signals. To ensure homogeneity in comparison of simulation and experimental results, the measured values of ambient temperature and thermal loads were input as look-up tables for the simulations. The load is connected to layer 6 of the hot tank and was applied as the value for the HT model parameter "Load-Layer". The data was logged with a change-of-value protocol and the logging dead-band was 2% of previous value.

Firstly, the time-series plots for three operational modes representing all the components are shown in Fig. 6 to Fig. 8. These plots express the dynamic interactions between the components evaluating their application in a system-wide simulation. The operation time of a component was also compared in experiment and simulation. Additionally, simulation of the internal control logic and dynamic or quasi-static behaviour of the components was analysed.

Secondly, two scatter plots expressing deviation of tank temperatures in a complex test scenario for summer and winter season relevant to system control are shown (Fig. 9a-b).

Fig. 6 expresses the results of a Summer Electricity Production (SEP) test. Here, the excess heat from the CHP is stored in the HT and is used to drive the AdC and cool down the CT. Similar to the experiment, a homogeneous initial temperature of 60.3 °C in the HT and 16.6 °C in the CT was used. The volume flows in the high,

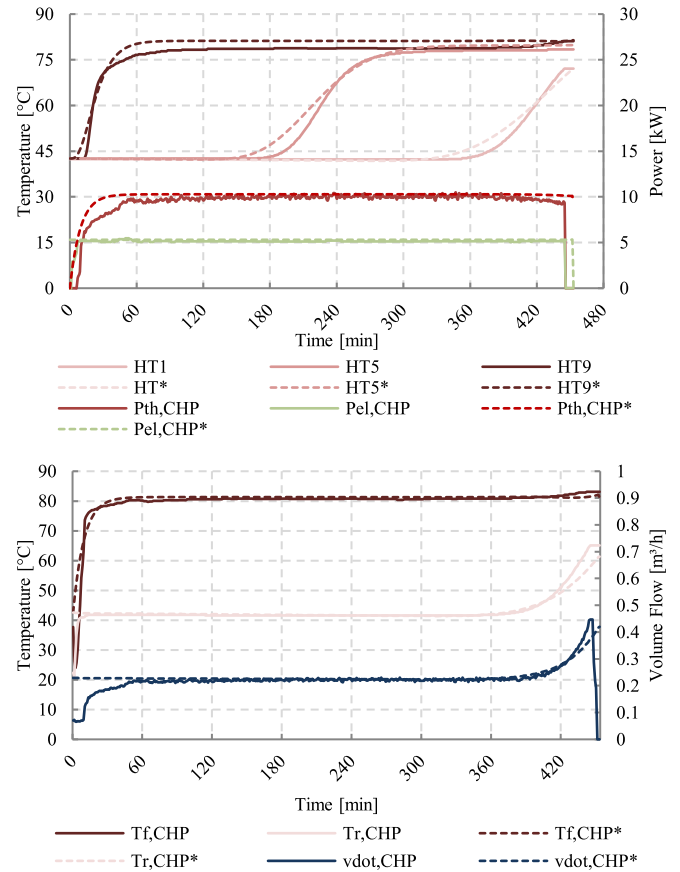


Fig. 7. Experimental and simulation results for the WEP mode. (a) HT temperatures and CHP powers. (b) CHP circuit temperatures and volume flow. Measured values (solid lines) and simulation results (*dashed lines).

medium and low temperature circuits were 1.3 m³/h, 4.2 m³/h and 1.7 m³/h respectively. In addition, a control signal of 1.5V was applied to the OC and the volume flow in the OC circuit was 4.7 m³/h. The AdC was switched on at time=0 min. To filter the noise in the measured data due to the periodic behaviour of the AdC, a 3-minute average of the circuit temperatures was utilised.

Two temperatures in the CT (CT1 at the bottom and CT4 at the top) are shown in Fig. 6(a). In addition, three temperatures in the HT (HT1, HT5 & HT7), with HT1 being at the bottom of the tank and HT7 corresponding to the outlet to the AdC are shown.

A deviation in the range 1 to 4K is observed and stratified cooling of the tanks replicates the real case. The periodic behaviour of the circuit temperatures is not observed in simulation results shown in Fig. 6(b), but consistent with the assumption, this is noticed to be damped in the tank temperatures. The AdC ran for 110 min in reality compared to the 114 min in simulation to achieve the set-point temperature of 12 °C for CT4.

In Fig. 7, the Winter Electricity Production (WEP) mode is simulated. Here the heat from CHP is stored in the HT and is used to cover the loads. Similar to the experiment, a homogeneous initial temperature of 43 °C in the HT was used. $P_{el,CHP(Nom)}$ and $P_{th,CHP(Nom)}$ were set to 5 kW_{el} and 10.2 kW_{th} respectively. $\eta_{el(Nom)}$ and $\eta_{th(Nom)}$ were set to 0.24 and 0.65 respectively, and the HCV_{Fuel} was set as 12 kWh/m³ assuming a gas CHP [40]. The CHP is switched on at time=0 min. Three temperatures in the HT (HT1, HT5 & HT9) with HT1 being at the bottom of the tank are shown in Fig. 7(a). A visual comparison shows temperature deviation in the range 1 to 6K in the HT temperatures. Thermal stratification behaviour is observed both in the experimental and simulation results. The main outputs of the CHP model are the feedline

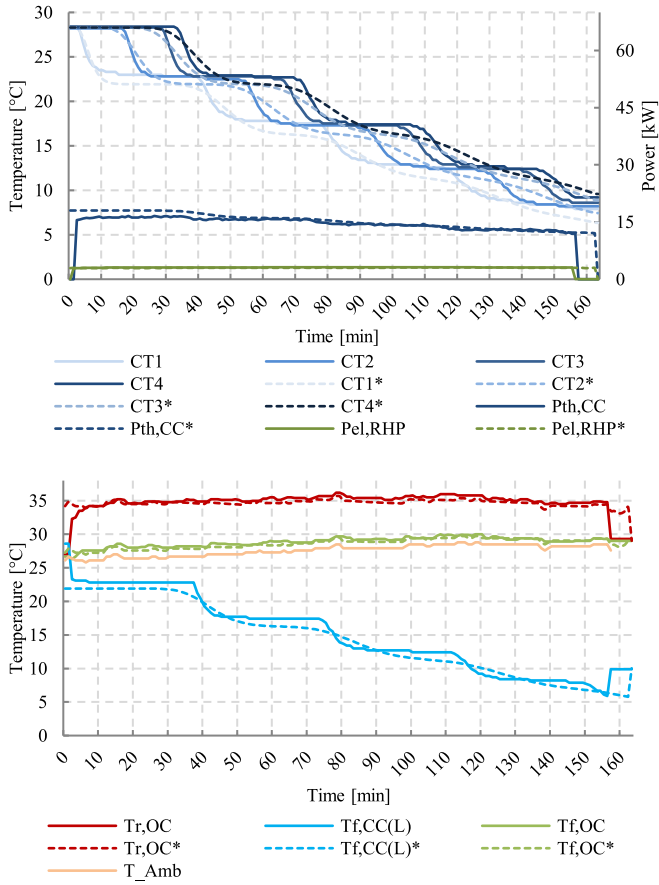


Fig. 8. Experimental and simulation results for the SEC mode. (a) CT temperatures and CC powers. (b) CC and OC circuit temperatures. Measured values (solid lines) and simulation results (*dashed lines).

temperature leaving the CHP $T_{f,CHP}$ and the volume flow of water \dot{V}_{CHP} which is controlled by the internal controller of the CHP to achieve a maximum possible feedline temperature as shown in Fig. 7(b). Visual analysis shows good accuracy for both outputs in the steady state. The dynamic behaviour of the CHP's thermal power $P_{th,CHP}$ during the start-up phase is also observed with a deviation of around 1 kW_{th} for the first 60 min and then a better fit is noticed in steady state. The simulated electric power $P_{el,CHP}^*$ shows a static response whereas the measured $P_{el,CHP}$ displays a quasi-static response. In the experiment the CHP turns off after 446 min and in the simulation after 453 min when HT1 reaches a set-point temperature of 72 °C. Although the thermal power and volume flow do not turn zero due to the dynamic equations, the formulation in (2) ensures that no mass flow occurs when the CHP is turned off and hence the HT is not affected.

The Summer Electricity Consumption (SEC) mode is simulated in Fig. 8. Here, the cooling power of the CC $P_{th,CC(L)}$ cools the CT down. Similar to the experiment a homogeneous initial temperature (condenser) and low (evaporator) temperature circuits were 2.65 m³/h and 2.45 m³/h respectively. In addition, a control signal of 10V was applied to the OC. The CC is switched on at time = 0 min. The four temperatures in the CT (CT1 to CT4 with CT1 at bottom) are shown in Fig. 8(a). Stratified cooling is simulated in the cold tank similar to the real case. The main outputs of the CC model are the chilled water temperature $T_{f,CC(L)}$, the cooling power $P_{th,CC(L)}$ and the electric consumption $P_{el,RHP}$ as shown in Fig. 8 (a & b). Additionally, the circuit temperatures of the OC model are shown. The OC receives a relatively steady 35 °C in its return line and cools

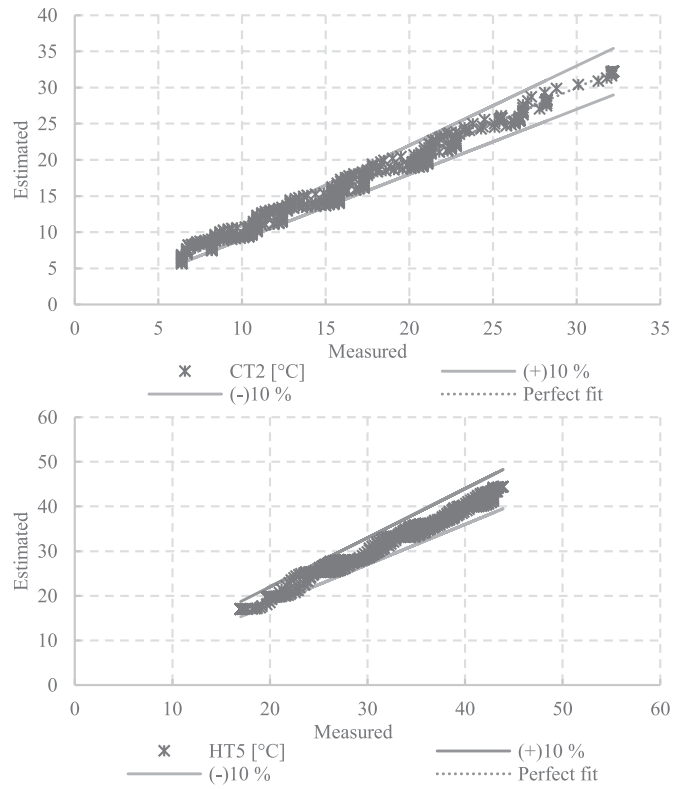


Fig. 9. Measured versus estimated results for the relevant tank temperatures. (a) Summer scenario. (b) Winter scenario.

it down to almost the ambient temperature T_{Amb} . This is in accordance to the fact that the OC is operating at its maximum speed due to the 10V signal. A visual comparison shows temperature deviation in the range of 1 to 2K in the two circuits and 1 to 4K in the tank temperatures. The cooling power and electric power consumption deviate by less than 1kW from the measured values.

The simulated values of cooling power and electric consumption, $P_{th,CC(L)}^*$ and $P_{el,RHP}^*$ display static behaviours and their measured values display quasi-static behaviours with a relatively short delay time of approx. 1 min. Another characteristic simulated is the part-load behaviour with decrease in cooling power as the CT temperatures decrease. In the experiment the machine ran for 158 min and in simulation for 163 min before turning off due to achieving set temperature of 10 °C for CT4.

The quality of the results are illustrated in more detail by comparing the measured and estimated tank temperature that is relevant in the case of the particular mode of operation as shown in Fig. 9. Since the tanks are the hydraulic and thermal interface between the source and load sides, these graphs facilitate a qualitative analysis of the complex physical interactions in the energy system.

Data was analysed for 8.5 h of CCM operation and 12 h of HP operation. It is seen that in most cases the estimated value of tank temperatures was within +/- 10% of the measured value. This is considered as an acceptable fit in the proposed qualitative analysis. A maximum deviation of approx. 15% is observed in the summer scenario at a lower temperature range and amounts to 1.5K. An inaccurate extrapolation of the curve fit models was observed in this region. The formation of thermoclines in the tanks during CC and HP operation is noticed in the wave-type illustration of the data points.

Table 5
Averaged evaluation metrics (standard deviation in brackets) from different tests.

	AdC		CHP		CC		HP	
	CT2	HT5	$T_{f,CHP}$	HT5	$T_{f,CC(L)}$	CT2	$T_{f,HP(H)}$	HT5
NRMSRE	0.12 (0.04)	0.24 (0.09)	0.07 (0.05)	0.05 (0.003)	0.06 (0.005)	0.03 (0.002)	0.16 (0.06)	0.03 (0.003)
r^2	0.96 (0.009)	0.79 (0.10)	0.85 (0.09)	0.98 (0.006)	0.96 (0.006)	0.98 (0.004)	0.91 (0.03)	0.98 (0.005)
MAE	0.37 (0.1)	2.5 (1.1)	1.2 (0.5)	1.17 (0.1)	1.04 (0.1)	0.706 (0.07)	3.8 (0.4)	0.67 (0.1)

For the quantitative analysis the following commonly used analytical metrics for HVAC simulation were chosen [16]:

$$NRMSRE = \sqrt{\frac{\sum_{i=1}^n \left(\frac{y_i - y_i^*}{y_{max} - y_{min}} \right)^2}{n}} \quad (32)$$

$$r^2 = \left(\frac{n \sum_{i=1}^n y_i y_i^* - \left(\sum_{i=1}^n y_i \right) \left(\sum_{i=1}^n y_i^* \right)}{\sqrt{n \left(\sum_{i=1}^n y_i^2 \right) - \left(\sum_{i=1}^n y_i \right)^2} \sqrt{n \left(\sum_{i=1}^n y_i^{*2} \right) - \left(\sum_{i=1}^n y_i^* \right)^2}} \right)^2 \quad (33)$$

$$MAE = \frac{\sum_{i=1}^n |y_i - y_i^*|}{n} \quad (34)$$

where,

NRMSRE - Normalised root mean squared relative error

r^2 - Coefficient of determination calculated as square of the Pearson product moment correlation coefficient

MAE- Mean absolute error

y_i - i^{th} measured value

y_i^* - i^{th} predicted value

\bar{y} - Arithmetic mean of measured values data set

\bar{y}^* - Arithmetic mean of predicted values data set

y_{max} - Maximum value of y in entire data set

y_{min} - Minimum value of y in entire data set

n - Number of data points

The fits are considered good when NRMSRE and MAE is close to zero and r^2 is close to one. The average value of evaluation metrics (standard deviation in brackets) from various tests of the main operational modes are shown in Table 5.

6. Discussion & conclusions

Deriving from existing methods in literature, a novel approach to develop optimal control orientated models of a complex poly-generation system was exhibited. An original experimental validation of these reduced parameter models was also presented.

Results in Fig. 6 to Fig. 8 shows a good fit of the tank temperatures in all different modes of operation demonstrating the ability of the individual models to work in tandem and simulate the complex interactions. The deviations noticed in Fig. 9 are for a short time-period and could be captured by further discretising the tank volume or including heat losses in the pipes. However, this will increase the number of system states. Ultimately, a balance between model size and accuracy must be made. The main outputs of the components are also simulated with sufficient accuracy as seen in circuit temperatures, powers, and volume flows in Fig. 6 to Fig. 8. The AdC model compromises on accuracy since the periodic behaviour and start-up cycle is not simulated, but it gains on simplicity which is needed for application in a MPC based supervisory controller. Furthermore, the static models for AdC and RHP are justified since the time constants of these components are typically smaller than 5 min. For plant operations having normally two to three start-up/shut-down cycles over an entire day, it is not indispensable to model their transient dynamics. The accuracy of

individual outputs could be improved further by using more high quality data for fitting the coefficients through optimal experimental design techniques or larger steady state datasets.

The NRMSRE, r^2 and MAE methods were used for quantitative analysis. Analytical values in Table 5 correspond to the good visual results however it is seen that no particular metric is suitable for the evaluation of all the variables and quantitative analysis should be performed in the context of the visual analysis based on the developer's criteria. This is consistent with existing conclusions [20]. The NRMSRE shows stable results and a value of less than 0.15 is considered as a good fit in this work since this also corresponds to a good visual fit and better r^2 (> 0.95) and MAE (< 1.2) values. During the analysis it was observed that r^2 is sensitive to the errors caused from mismatch of time-series or when neglecting dynamics of components, but it is suitable for evaluating tank temperatures. The largest MAE of 3.8K is in the HP scenario and is negligible considering the tolerance that is acceptable in such complex thermal systems and neglecting effects of measurement errors and thermal losses. The proposed models of AdC, CHP, and HP are lesser accurate compared to models in literature but also have 10, 3, and 5 parameters lesser respectively (Table 3). It must be reiterated that they still have enough accuracy for the system wide simulation which was evident from the fact that maximum MAE for totalelectricity balance amongst all scenarios was only 1.0 kWh_{el}. And the maximum MAE in operational costs (including fuel consumption, auxiliary consumption) amongst all scenarios was 0.02 €/kWh_{el}.

The quantitative and qualitative arguments presented above support the application of the proposed models for system-level simulation of polygeneration plants with multiple components and storages. Additionally, since the limited model errors can be alleviated within the fifteen minutes MPC loop and the lesser complexity and continuous differentiability can be positively exploited, this model set shows promising potential for application in optimal scheduling with respect to the energy market. However, they are rendered unsuitable for grid voltage or frequency management based optimal scheduling problems. Furthermore, as the models use readily available data for parameter identification and they reflect internal control and part-load aspects of components, they satisfy the desired characteristics for real-world applications.

In future work, this model set will be utilised within a mixed-integer optimal control problem formulation for economic-MPC of the system. Further simplification of the models will be investigated by; (a) substituting the NTU- ϵ method for OC by variable expressions of the T_{Amb} , (b) substituting the fan-affinity laws with a variable expression of the RPM and (c) reducing the second order fits to first order fits. Subsequently the building automation and control architecture will be extended to fit the coefficients of regression in real-time for creating a self-learning model set.

Author statement

Each named author has substantially contributed to conducting the underlying research and drafting this manuscript. The contributions were in conceiving and designing the experiments, performing the experiments, analysing and interpreting the data, contributing materials and analysis tools, and writing the paper.

Declaration of Competing Interest

Each named author has substantially contributed to conducting the underlying research and drafting this manuscript. Additionally, to the best of our knowledge, the named authors have no conflict of interest, financial or otherwise. The authors declare that they have no known competing financial interests or personal relationships that could have appeared to influence the work reported in this paper.

Acknowledgements

The authors are grateful to the [Reiner Lemoine Stiftung \(1581440000956\)](#), Alexander von Humboldt Stiftung, E-Werk Mittelbaden Innovations Fond, the State Ministry of Baden-Wuerttemberg for Sciences, Research and Arts ([Az: 22-7533.-30-20/9/3](#)) and the Forschungsallianz Oberrhein for their support.

Supplementary materials

Supplementary material associated with this article can be found, in the online version, at [doi:10.1016/j.enbuild.2019.109725](https://doi.org/10.1016/j.enbuild.2019.109725).

References

- [1] M. Jradi, S. Riffat, Tri-generation systems: energy policies, prime movers, cooling technologies, configurations and operation strategies, *Renew. Sustain. Energy Rev.* 32 (2014) 396–415.
- [2] H. Cho, A.D. Smith, P. Mago, Combined cooling, heating and power: a review of performance improvement and optimization, *Appl. Energy* 136 (Dec. 2014) 168–185.
- [3] V. Andiappan, State-Of-The-Art review of mathematical optimisation approaches for synthesis of energy systems, *Process Integr. Optim. Sustain.* 1 (3) (Oct. 2017) 165–188.
- [4] H. Cho, P.J. Mago, R. Luck, L.M. Chamra, Evaluation of CCHP systems performance based on operational cost, primary energy consumption, and carbon dioxide emission by utilizing an optimal operation scheme, *Appl. Energy* 86 (12) (Dec. 2009) 2540–2549.
- [5] J.S. Kim, T.F. Edgar, Optimal scheduling of combined heat and power plants using mixed-integer nonlinear programming, *Energy* 77 (Dec. 2014) 675–690.
- [6] M. Liu, Y. Shi, F. Fang, Combined cooling, heating and power systems: a survey, *Renew. Sustain. Energy Rev.* 35 (Jul. 2014) 1–22.
- [7] J. Ortega, J.C. Bruno, A. Coronas, Operational optimisation of a complex tri-generation system connected to a district heating and cooling network, *Appl. Therm. Eng.* 50 (2) (2013) 1536–1542.
- [8] H. Dagdougui, R. Minciardi, A. Ouammi, M. Robba, R. Sacile, Modeling and optimization of a hybrid system for the energy supply of a 'Green' building, *Energy Convers. Manag.* 64 (2012) 351–363.
- [9] P.A. Sawant, J. Pfaffert, Experimental investigation of a real-life microscale trigeneration system using adsorption cooling, reversible heat-pump and a co-generation unit, in: 7th IC- EPSMSO, 2017, pp. 155–165.
- [10] A. Lefort, R. Bourdais, G. Ansanay-Alex, H. Guéguen, Hierarchical control method applied to energy management of a residential house, *Energy Build* 64 (Sep. 2013) 53–61.
- [11] Z. Zhou, P. Liu, Z. Li, E.N. Pistikopoulos, M.C. Georgiadis, Impacts of equipment off-design characteristics on the optimal design and operation of combined cooling, heating and power systems, *Comput. Chem. Eng.* 48 (Jan. 2013) 40–47.
- [12] V. Chandan, A. Do, B. Jin, F. Jabbari, J. Brouwer, I. Akrotirianakis, Modeling and optimization of a combined cooling, heating and power plant system, in: American Control Conference, 2012, pp. 3069–3074.
- [13] M. Trčka, J.L.M. Hensen, Overview of HVAC system simulation, *Autom. Constr.* 19 (2) (2010) 93–99.
- [14] J. Široký, F. Oldewurtel, J. Cigler, S. Prívra, Experimental analysis of model predictive control for an energy efficient building heating system, *Appl. Energy* 88 (9) (Sep. 2011) 3079–3087.
- [15] A. Wächter, L.T. Biegler, On the implementation of an interior-point filter line-search algorithm for large-scale nonlinear programming, *Math. Program.* 106 (1) (Mar. 2006) 25–57.
- [16] A. Afram, F. Janabi-Sharifi, Gray-box modeling and validation of residential HVAC system for control system design, *Appl. Energy* 137 (2015) 134–150.
- [17] T. Bohlin, A case study of grey box identification, *Automatica* 30 (2) (Feb. 1994) 307–318.
- [18] B. Sohlberg, Grey box modelling for model predictive control of a heating process, *J. Process Control* 13 (2003) 225–238.
- [19] A. Afram, F. Janabi-Sharifi, Black-box modeling of residential HVAC system and comparison of gray-box and black-box modeling methods, *Energy Build* 94 (May 2015) 121–149.
- [20] N. Fumo, M.A. Rafe Biswas, Regression analysis for prediction of residential energy consumption, *Renew. Sustain. Energy Rev.* 47 (Jul. 2015) 332–343.
- [21] M. Diehl, "Lecture notes on 'Systemtheorie und regelungstechnik,'" no. August. Freiburg, 2014.
- [22] P. Fritzson, Principles of Object-Oriented Modeling and Simulation With Modica 3.3: a Cyber-Physical Approach, John Wiley & Sons, 2014.
- [23] S. Li, J.Y. Wu, Theoretical research of a silica gel-water adsorption chiller in a micro combined cooling, heating and power (CCHP) system, *Appl. Energy* 86 (6) (2009) 958–967.
- [24] M. Schickanz, T. Núñez, Modelling of an adsorption chiller for dynamic system simulation, *Int. J. Refrig.* 32 (4) (2009) 588–595.
- [25] H. Ren, W. Gao, Y. Ruan, Optimal sizing for residential CHP system, *Appl. Therm. Eng.* 28 (5–6) (Apr. 2008) 514–523.
- [26] H. Cho, R. Luck, S.D. Eksioğlu, L.M. Chamra, Cost-optimized real-time operation of CHP systems, *Energy Build* 41 (4) (Apr. 2009) 445–451.
- [27] H. Jin, J.D. Spitler, A parameter estimation based model of water-to-water heat pumps for use in energy calculation programs, *ASHRAE Trans.* 108 (PART 1) (2002) 3–17.
- [28] V. Lemort, J. Lebrun, and C. Felsmann, "Testing and validation of simulation tools of HVAC mechanical equipment including their control strategies part III: validation of an air-cooled chiller model," in *IBPSA Building Simulation*, 2009, no. 2002, pp. 1121–1128.
- [29] U. Eicker, Storage modelling, in: *Solar Technologies for Buildings*, John Wiley & Sons, Stuttgart, 2006, pp. 97–103.
- [30] Y. Ma, F. Borrelli, B. Hency, A. Packard, S. Bortoff, Model predictive control of thermal energy storage in building cooling systems, in: 48th IEEE Conference on Decision and Control (CDC), 2009, pp. 392–397.
- [31] Y. Zhao, Y. Lu, C. Yan, S. Wang, MPC-based optimal scheduling of grid-connected low energy buildings with thermal energy storages, *Energy Build* 86 (2015) 415–426.
- [32] D.I. Hidalgo Rodriguez, L. Spitalny, J. Myrzik, M. Braun, Development of a control strategy for mini CHP plants for an active voltage management in low voltage networks, in: 3rd IEEE PES Conference, 2012, pp. 1–8.
- [33] J. Seifert, Mikro BHKW Systeme Für Den Gebäude Bereich, VDE Verlag GmbH, Berlin, 2013.
- [34] G. Salvalai, Implementation and validation of simplified heat pump model in IDA-ICE energy simulation environment, *Energy Build* 49 (2012) 132–141.
- [35] A.L. Facci, L. Andreassi, S. Ubertini, Optimization of CHCP (combined heat power and cooling) systems operation strategy using dynamic programming, *Energy* 66 (2014) 387–400.
- [36] G.P. Henze, B. Biffar, D. Kohn, M.P. Becker, Optimal design and operation of a thermal storage system for a chilled water plant serving pharmaceutical buildings, *Energy Build* 40 (6) (Jan. 2008) 1004–1019.
- [37] D.W. Wu, R.Z. Wang, Combined cooling, heating and power: a review, *Prog. Energy Combust. Sci.* 32 (5–6) (2006) 459–495.
- [38] A. Bürger, C. Zeile, A. Altmann-Dieses, S. Sager, M. Diehl, An algorithm for mixed-integer optimal control of solar thermal climate systems with MPC-Capable runtime, in: 2018 Eur. Control Conf. ECC 2018, 2018, pp. 1379–1385.
- [39] T.L. Bergman, F.P. Incropera, D.P. DeWitt, A.S. Lavine, Fundamentals of Heat and Mass Transfer, John Wiley & Sons, 2011.
- [40] P. Sawant, J. Pfaffert, C. Felsmann, Quasi-First-Principle based grey-box modelling of microscale trigeneration systems for application in automatic control, *IFAC-PapersOnLine* 51 (28) (Jan. 2018) 690–695.
- [41] a.Campos Celador, M. Odriozola, J.M. Sala, Implications of the modelling of stratified hot water storage tanks in the simulation of chp plants, *Energy Convers. Manag.* 52 (8–9) (2011) 3018–3026.
- [42] R. De Césaró Oliveski, A. Krenzing, H. a. Vielmo, Comparison between models for the simulation of hot water storage tanks, *Sol. Energy* 75 (2) (2003) 121–134.
- [43] G. Streckiene, V. Martinaitis, P. Vaitiekunas, Simulation of thermal stratification in the heat storage for CHP plant, in: 8th IC- Env. Eng., 2011, pp. 812–819.